

Inferring HIV escape rates from multi-locus genotype data

Taylor A. Kessinger¹, Alan S. Perelson² and Richard A. Neher¹

¹Max Planck Institute for Developmental Biology, 72076 Tübingen, Germany, and ²Theoretical Biology and Biophysics, Los Alamos National Laboratory, Los Alamos, NM 87545, USA

(Dated: August 29, 2020)

Cytotoxic T-lymphocytes (CTLs) recognize viral protein fragments displayed by major histocompatibility complex (MHC) molecules on the surface of virally infected cells and generate an anti-viral response that can kill the infected cells. Virus variants whose protein fragments are not efficiently presented on infected cells or whose fragments are presented but not recognized by CTLs therefore have a competitive advantage and spread rapidly through the population. We present a method that allows a more robust estimation of these escape rates from serially sampled sequence data. The proposed method accounts for competition between multiple escapes by explicitly modeling the accumulation of escape mutations and the stochastic effects of rare multiple mutants. Applying our method to serially sampled HIV sequence data, we estimate rates of HIV escape that are substantially larger than those previously reported. The method can be extended to complex escapes that require compensatory mutations. We expect our method to be applicable in other contexts such as cancer evolution where time series data is also available.

During the first few months of HIV infection, the HIV genome typically undergoes a series of rapid amino acid substitutions that reduce immune pressure by cytotoxic T-lymphocytes (CTLs); this process is referred to as CTL escape (McMichael *et al.*, 2009). The substitutions arise by random mutation and spread through the viral population by impairing either the presentation of viral epitopes on the cell surface or the recognition of the viral epitope by T-cell receptors. Avoiding recognition is an obvious benefit to the mutant virus, but escape mutations can interfere with processes necessary for virus replication and infection and thereby reduce the virus’ intrinsic fitness (Fernandez *et al.*, 2005; Ganusov *et al.*, 2011; Li *et al.*, 2007; Seki and Matano, 2012). The rate at which escape variants displace the founder sequences depends on both “avoided killing” and the fitness cost. To quantify the role of individual CTL clones in controlling the viral population and the fitness costs associated with escape mutations, one would like to infer the escape rate associated with the individual mutations from serially sampled sequence data (Asquith *et al.*, 2006; Ganusov *et al.*, 2011).

With a single escape mutation and dense, deeply sampled data, the escape rate can simply be estimated by fitting a logistic curve to the time course of the mutation’s frequency (Asquith *et al.*, 2006; Ganusov *et al.*, 2011). The logistic curve has two parameters: the growth or escape rate and the frequency at the initial time point. In many cases, however, the data obtained from infected patients are scarce, and estimating two parameters reliably from the data is not possible since one needs at least two time points at which the mutation is at intermediate frequency between 0 and 1 (Ganusov *et al.*, 2011). Figure 1 shows an example of such time series sequence data from CTL escape during early HIV infection. Time points are far apart and the sampling depth is low. Furthermore, it is not the case that only a single escape mutation is observed; rather, several mutations rapidly emerge in

different places in the viral genome (Goonetilleke *et al.*, 2009; Salazar-Gonzalez *et al.*, 2009). Multiple escapes imply immune pressure on many epitopes. Since the viral population and its mutation rate are large (Mansky and Temin, 1995; Perelson *et al.*, 1996), these different escape mutations will arise almost simultaneously. Initially, these escape mutations exist in the population as single mutant genomes until they are combined into multiple mutants by recurrent mutation or recombination (Ganusov *et al.*, 2013; Leviyang, 2013). The competition between viral variants affects the trajectories of individual escape mutations, so estimating their intrinsic growth rate by logistic fitting is not accurate. This competition is known as “clonal interference” in population genetics. The degree of competition between genotypes depends on the population size, the mutation rate, and the recombination rate in HIV populations. The latter-most is rather low (Batorsky *et al.*, 2011; Neher and Leitner, 2010), and two strongly selected mutations in a large population are more likely combined by additional de novo mutation than recombination with another rare single mutation.

Here, we develop a strategy for inference that allows one to obtain robust escape rate estimates from the scarce data typical of studies of CTL escape. The inference is based on explicit modeling of the process of mutation accumulation in the founder sequence. Thereby, we exploit constraints imposed by the underlying dynamics of mutation and selection in the high dimensional space of possible genotypes.

Despite the large number of possible genomes that can be formed from different combinations of escape mutations, we typically observe one or two dominant genotypes at a time – at least during the first few month of the infection. Furthermore, these genotypes dominate only transiently and are quickly displaced by genotypes with an even greater number of escape mutations; see Fig. 1. These observations agree with results from ref. (Silva,

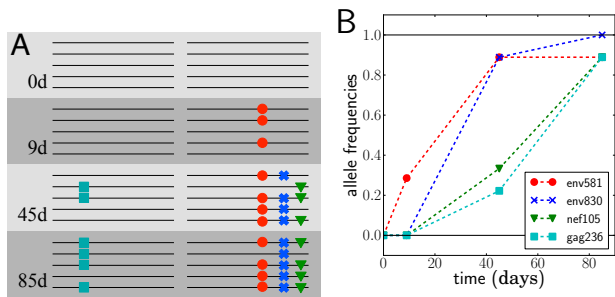


Figure 1 Escape from T-cell mediated immunity. The virus population in patient CH58 quickly acquires four substitutions. Panel A shows a sketch of genotypes at the first 4 escape mutations, observed at different times; see (Goonetilleke *et al.*, 2009; Salazar-Gonzalez *et al.*, 2009) for the actual data. Panel B shows the frequencies of the mutations in samples of size 7 at day 9 and size 9 at days 45 and 85.

2012), where a model of acute HIV infection was used to show that strongly selected escape mutations fix sequentially. Note that we don't assume a particular sequence of dominant genotypes a priori. Instead, we observe a sequence of dominant genotypes and try to infer the evolutionary scenario that most likely gave rise to this sequence of genotypes. While we model only these genotypes, many minor variants certainly exist. But only those dominant variants that are likely to give rise to the future populations need to be modeled accurately. Later in infection, the viral population is very diverse and cannot be analyzed using our method.

Given a data set from early infection, it is typically straightforward to define a series of dominant genotypes that likely have arisen through step-wise accumulation of mutations. Note that most likely all escape mutations constantly arise in different combinations, but typically only one combination rises quickly enough to dominate the population. This dominant genotype is then in most cases the source for the next dominant genotype. Later in infection, however, recombination is sufficiently frequent that no dominant genotype exists and mutations can spread simultaneously.

In Ganusov *et al.* (Ganusov *et al.*, 2013), a framework for multi-locus modeling of CTL escape is presented. Building on this framework, we explicitly model the transition from one dominant genotype to another, which is a good approximation of the dynamics for rapid CTL escape in acute infection. The restriction to dominant genotypes captures the interference between escapes at different epitopes while avoiding the need to solve the full multi-locus problem.

We will first define a model of the dynamics of escape mutations. This model serves a two-fold purpose: it defines the parameters we would like to estimate from the data and provides us with a computational tool to investigate how the accuracy of the inference depends on sampling depth and frequency, as well as how sensitively

it depends on the values of parameters such as mutation rates or the population size. We reanalyze existing CTL escape data and find that accounting for multi-locus effects in a finite population results in higher estimates of the escape rates.

I. RESULTS

A. Model

In the majority of sexually transmitted HIV infections, a single “transmitted/founder” virus initiates the new infection resulting in an initially homogeneous viral population (Keele *et al.*, 2008; Salazar-Gonzalez *et al.*, 2009). However, as HIV replicates in its new host, mutations accumulate. Mutations within or in proximity to CTL epitopes can reduce immune pressure by facilitating the avoidance of CTL recognition. While one often observes several escape mutations within a single epitope (Fischer *et al.*, 2010; Henn *et al.*, 2012), we do not differentiate between different mutations within the same epitope and model L epitopes that can be either be mutant or wild-type. Assuming that the escape at multiple epitopes has additive effects, ϵ_j , the growth rate (birth rate minus death rate) of a genotype is given by

$$F(g, t) = F_0(t) + \sum_i \epsilon_i s_i \quad (1)$$

where $g = \{s_1, \dots, s_L\}$ specifies the genotype. Here, $s_i = 0$ corresponds to a wild-type epitope at locus i , whereas $s_i = 1$ signifies escape at that epitope. $F_0(t)$ accounts for a genotype independent modulation of the growth rate. The latter could, for example, be due to variable numbers of target cells (Ganusov and De Boer, 2006; Petravic *et al.*, 2008a). $F_0(t)$ controls the total population size, while the differences between genotypes are accounted for by $\sum_i \epsilon_i s_i$ and result in differential amplification of some genotypes over others. The ϵ_i are the escape rates that we would like to estimate from the data and should be interpreted as the net effect of avoided killing and the possible fitness costs associated with the mutation; see *e.g.* Ganusov *et al.* (Ganusov *et al.*, 2013). The fitness costs are modulated by the overall growth rate of the viral population and could therefore be slightly time dependent. We neglect this complication.

Within our model, mutations arise at a rate μ per base per generation. This rate can be epitope dependent. Motivated by the frequent template switching of HIV reverse transcriptase (Levy *et al.*, 2004), our general model of the HIV population includes recombination, which is assumed to occur with rate r . In the event of recombination, all L epitopes are reassorted, but an explicit genetic map could be implemented as well.

We implemented our model as a computer simulation in Python using the population genetic library FFPopSim (Zanini and Neher, 2012). The simulation stores

the population $n(g, t)$ of each of the 2^L possible genotypes. In each generation, the expected changes of the $n(g, t)$ due to mutation, selection, and recombination are calculated. The population of the next generation is then sampled from the expected genotype frequencies $\gamma(g, t) = n(g, t)/N$. The size of the population, N , can be set at will each generation. In this way, up to 15 epitopes can be simulated for 1000 generations within seconds to minutes.

A typical realization of the population dynamics is shown in Fig. 2, where we have assumed a generation time of one day. As expected, the population is dominated by one genotype at a time. Furthermore, the mutations accumulate in decreasing order of escape rate, and the new dominant genotype arises from the previous by incorporation of the mutation with the largest escape rate available. There are, however, many minority genotypes which are rarely observed. Figure 2C shows the frequencies on a logarithmic scale, where the minor variants are visible. We use these simulations to test the accuracy and robustness of the inference procedure developed below.

Of the many possible genotypes that are present at any moment, only a small fraction is likely to be observed in a small sample and to be relevant in the future. Simulations and data suggest that the dominant genotypes accumulate mutations one by one – this greatly simplifies the task of estimating escape rates from the data. Instead of considering the dynamics of all possible genotypes (2^L), we will restrict the inference to a chain of genotypes, each containing one additional mutation compared to its predecessor.

The best estimates for the HIV generation time are $d = 2$ days (Markowitz *et al.*, 2003), while estimates of escape rates are typically given in units of inverse days rather than generations. For simplicity, we simulate our model assuming one generation per day and state all rates in units of 1/day. Our results are insensitive to the choice of the generation time. Doubling the generation time has similar effects to dividing the population size by 2, as this keeps the strength of genetic drift constant.

B. Inferring the escape rates

Suppose we have obtained sequence samples of size n_i at different time points t_i and each of these samples consists of different genotypes g present in $k(g, t_i)$ copies. If the actual frequencies of the those genotypes at different times are $\gamma(g, t_i)$, the probability of obtaining the sample at t_i is given by the multinomial distribution

$$P(\text{sample}) = \frac{n_i!}{\prod_g k(g, t_i)!} \prod_g \gamma(g, t_i)^{k(g, t_i)} \quad (2)$$

If the underlying dynamics were deterministic, the frequencies $\gamma(g, t)$ would be unique functions of the model parameters we want to estimate. In that case we could

use Bayes’ theorem, choose suitable priors, and determine the posterior distribution of the parameter values. However, both the model and the actual viral dynamics are stochastic, and “replaying” the history would result in different trajectories. Furthermore, most of the 2^L possible genotypes remain unobserved. This leaves us with the choice of either some type of approximate Bayesian computation that compares repeated simulations of the model with appropriate summary statistics (Sunner *et al.*, 2013) or a reduced description of only the observed genotypes, with the stochasticity captured by nuisance parameters (Basu, 1977).

We opt for the latter and model only those genotypes that dominate the population. We label these genotypes by the number of escape mutations they carry, e.g., g_1 carries the first escape mutations, g_2 the first and the second, and so forth. The frequency of a genotype is affected by stochastic forces only while it is very rare. If the genotype is favored, it will rapidly rise to high frequency, and the stochastic effects will no longer be relevant. It is therefore convenient to summarize the stochastic behavior by the time, τ , at which its frequency crosses the threshold to essentially deterministic dynamics. Since the dynamics is deterministic after this “seed time”, all the (unobserved) stochasticity can be accounted for by an appropriate choice of the seed time (Desai and Fisher, 2007; Kepler and Perelson, 1995). For each of the dominant escape variants, g_j , with $j = 1$ to $j = L$ escaped epitopes, we define a seed time τ_j to accommodate the stochastic aspects of the escape dynamics.

After crossing the deterministic threshold, the population frequencies of the dominant genotypes evolve according to

$$\dot{\gamma}_j(t) = F(g_j, t)\gamma_j(t) + \mu[\gamma_{j-1}(t) - \gamma_j(t)] \quad (3)$$

if $t > \tau_j$. Conversely, $\gamma_j(t) = 0$ for $t < \tau_j$. The growth rate $F(g_j, t)$ of genotype j is the sum of the escape rates ϵ_k of the epitopes $k = 1, \dots, j$ and the density regulating part $F_0(t)$; compare to Eq. (1). The escape rates are what we would like to estimate. The seed time, τ_j , corresponds to the time at which a genotype with all escape mutations up to mutation j first establishes¹. At the seed time, we initialize the genotype frequency at $\gamma_j(\tau_j) = N^{-1}$. If seed times are chosen appropriately, this model provides a very accurate description of the frequency dynamics of the dominant genotypes in the full stochastic model; see Fig. 3.

At face value, the deterministic model has two parameters per epitope – one escape rate and one seed time. The seed times, however, are quite strongly constrained

¹ There is a brief period after the initial production of the mutation during which the dynamics is stochastic and the initial mutant establishes only with a probability roughly equal to ϵd , where $d = 2$ days is the generation time (Markowitz *et al.*, 2003). However, we find $\epsilon d \approx 1$ and ignore this complication.

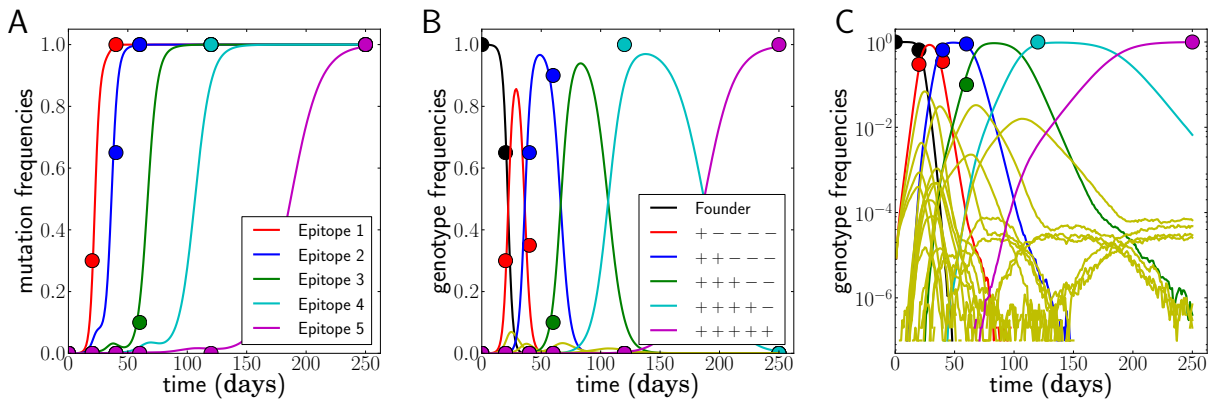


Figure 2 Example of simulated escape mutations spreading through the population. (A) Even though all epitopes are targeted from $t = 0$, escape mutations spread sequentially. The mutation frequency in a sample of size 20 at different time points is indicated by colored dots. (B) The rising mutation frequencies are associated with the rise and fall of multilocus genotypes. The founder virus is first replaced by a dominant single mutant, which itself is replaced by a double mutant and so forth. Note, however, that the virus population explores many combinations of mutations but that these minor variants never reach appreciable frequency. This is best seen in panel (C), where all 32 genotype frequencies are shown on a logarithmic scale. These rare variants are rarely sampled, and their noisy dynamics suggests that little information can be gained from them. Here, $N = 10^7$, $\mu = 10^{-5}$, and $r = 0$ and escape rates are $\epsilon_j = 0.5, 0.4, 0.25, 0.15, 0.08$ per day.

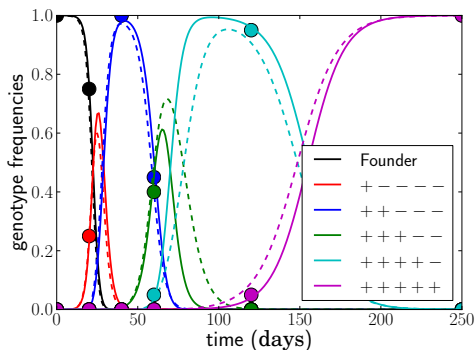


Figure 3 The deterministic model parameterized by seed times τ_j for the L dominant genotypes and the escape rates of epitopes ϵ_i (solid lines) captures the dynamics of the stochastic model accurately (dashed lines). The trajectories (and seed times) vary from run to run. In this run, $N = 10^7$, $\mu = 10^{-5}$, and $r = 0$ and the escape rates are $\epsilon_j = 0.5, 0.4, 0.25, 0.15, 0.08$ per day.

by basic facts of the evolutionary dynamics. The genotype g_j carrying mutations $i = 1, \dots, j$ arises with rate $\mu N(t) \gamma_{j-1}(t)$ from the genotype g_{j-1} carrying only $j-1$ mutations. This means it is unlikely that genotype j arises early while $\gamma_{j-1}(t)$ is still very small. However, once the previous genotype $j-1$ is common, genotype j is produced frequently. The distribution of the time at which the first copy of genotype j arises is given by the product of the rate of production and the probability that it has not yet been produced. The latter is the negative exponential of the integral of the production rate

up to this point. Hence, the distribution of the seed time τ_j , given the trajectory of the previous genotype γ_{j-1} , is given by

$$Q(\tau_j | \gamma_{j-1}(t)) \approx \mu N(\tau_j) \gamma_{j-1}(\tau_j) e^{-\mu \int_0^{\tau_j} N(t) \gamma_{j-1}(t) dt}. \quad (4)$$

Since the $\gamma_j(t)$ are uniquely specified by $\{\tau_k, \epsilon_k\}_{k=1, \dots, L}$, we can write the posterior probability of the parameters as

$$P(\{\epsilon_j, \tau_j\}) \propto \prod_i P(\text{sample}_i | \Theta) \prod_j Q(\tau_j | \Theta) U(\epsilon_j), \quad (5)$$

where $\Theta = \{\epsilon_k, \tau_k\}_{k=1 \dots L}$ and $U(\epsilon_j)$ is our prior on the escape rates. We employ a Laplace prior $U(\epsilon) = \exp(-\Phi \epsilon)$ parameterized by Φ favoring small escape rates. The prior regularizes the search for the minimum and results in conservative estimates of escape rates.

C. Obtaining maximum likelihood estimates

Finding the set of escape rates and seed times that maximizes the posterior probability can be difficult due to multiple maxima and ridges in the high dimensional search space, and uncertainty remains. To ensure that the global optimum will be reliably discovered, we exploit the sequential nature of the dynamics and use the fact that earlier escapes strongly affect the timing of the later ones, but not vice versa. Thus adding genotypes with an increasing number of mutations one at a time results in a reasonable initial guess on top of which a global true multi-locus search can be performed.

We have implemented such a search in Python, while the computationally expensive calculation of the poste-

rior probability is implemented in C. The code infers parameters as follows:

- Fit the first escape assuming $\tau_1 = 0$ by a simple one dimensional minimization. This assumes that single mutants are already present in the population, consistent with the large viral population size present by the time a patient has been identified as HIV-1 infected (Coffin, 1995; Perelson *et al.*, 1997).
- Add additional epitopes successively by mapping the entire two-dimensional posterior distribution $P(\epsilon_j, \tau_j)$ at fixed $\{\epsilon_k, \tau_k\}$ for $k < j$. This step is illustrated in Fig. 4A.
- Refine the estimates through local optimization via gradient descent, Monte Carlo methods, or local exhaustive search. The resulting parameters and trajectories are shown for one example in Fig. 4B.
- Generate posterior distributions by Markov chain Monte Carlo (MCMC).

This procedure is described in more detail in the methods section. Fitting a five epitopes takes on the order of a minute on one 2011 desktop machine (Apple iMac i7 2.93 GHz). Generating the local posterior distribution by MCMC takes roughly 20 minutes for 10^6 steps.

D. Comparison to simulated data

To evaluate the accuracy and reliability of our inference scheme, we performed true multi-locus stochastic simulations using FFPopSim (see methods) and sampled genotypes from the simulation at a small number of time points. Time points and sample sizes were chosen to mimic patient data. We then inferred parameters from this “toy” data and compared the result to the actual values. When interpreting these comparisons, it is important to distinguish two sources of error. First, limited sample size and sampling frequency will incur errors due to inaccurate estimates of the actual genotype frequencies from the sample. The second source of uncertainty is an inappropriate choice of model or model parameters. Such inappropriate model choices might include wrong estimates of the population size or mutation rates, the presence or absence of recombination, or time variable CTL activity.

We generate data assuming escape rates $\epsilon_j = 0.5, 0.4, 0.25, 0.15, 0.08$ per day and sample the population on days $t_i = 0, 20, 40, 60, 120, 250$. An example of such samples is shown in Fig. 2. Note that each genotype is typically only sampled at a single data point; it easily happens that a genotype is hardly seen at all. We therefore expect all inferences to be quite noisy as is the case with patient data.

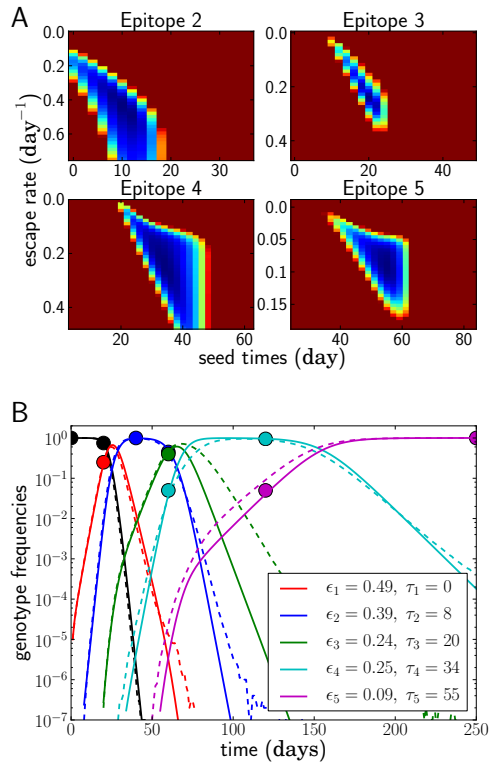


Figure 4 Adding epitopes one by one is a feasible and reliable fitting strategy. Assuming we know the population was homogeneous at $t = 0$, there is only one free parameter for the first epitope, which is easily determined. For all subsequent epitopes, we need to determine the seed time τ_j and the escape rate ϵ_j . In panel A, the negative log posterior probability of these parameters is shown for each of the epitopes. The surface typically exhibits a single minimum. Panel B shows the genotype frequencies of the founder virus and the dominant escape variants (solid lines: model fit, dashed lines: actual simulated trajectories). The estimated escape rates of individual epitopes and the seed times of genotypes containing all escape mutations up to j are given in the legend. Only the samples indicated by balls (20 sequences at each time point) were used for the estimation. In this run, $N = 10^7$, $\mu = 10^{-5}$, $r = 0$, and the escape rates $\epsilon_j = 0.5, 0.4, 0.25, 0.15, 0.08$ per day.

1. Sample size and sampling frequency dependence

With more frequent and deeper sampling, inferring the model parameters is expected to become simpler. Indeed, as soon as each genotype is sampled more than once at intermediate frequency, one can estimate its growth advantage simply from its rate of increase. This is the rationale behind previous studies such as (Asquith *et al.*, 2006; Ganusov *et al.*, 2011). In many data sets, however, this condition is not met. By constraining the seed time based on the evolutionary trajectory of the previous escape, our method is able to produce a more accurate reconstruction of parameters with less data.

Figure 5 shows the estimates obtained as a function of the sampling frequency and sample size. Increasing the sample size improves the estimates only moderately, while increasing the sampling frequency leads to substantial improvements.

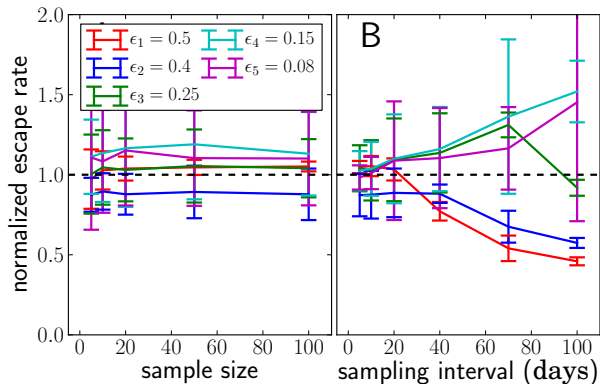


Figure 5 The dependence of the accuracy of inference on sample sizes (panel A) and sampling intervals (panel B). The actual normalized escape rate is 1.0 and is shown by the dashed line. Sample size only moderately affects the accuracy, while sparse sampling (every 40 days in this example) leads to serious loss of accuracy. Sample size is $n = 20$ when sample intervals are varied, and sampling times are as illustrated in Fig. 2 when sample size is varied. The plots show the mean \pm one standard deviation. The actual values of the escape rates simulated are shown in the legend (same on both panels). In each run, $N = 10^7$, $\mu = 10^{-5}$, and $r = 0$. Mean and standard deviation at each point are calculated from 100 independent simulations.

2. Model deviations

The population size and the mutation rate explicitly enter our model through the seed time prior, but we rarely know these numbers accurately. Hence we need to understand how inaccurate assumptions affect our estimates. If we assume that $N\mu$ is larger than it really is, our inference method will favor seeding subsequent genotypes too early, which in turn results in erroneously small estimates of escape rates. We varied N and μ and observed the expected effect on the estimates as shown in Fig. 6. The dependence on μ is stronger than that on N , since the effect of a larger population size is partly canceled by the longer time necessary to amplify the novel mutation to macroscopic numbers. However, even the dependence on μ is rather weak, and changing μ ten-fold only changes estimates of escape rates by $\pm 50\%$. The underlying reason is that the seed times depend primarily on the logarithm of $N\mu$. $Q(\tau_j | \gamma_{j-1}(t))$ (see Eq. (4)) peaks when $N\mu\gamma_{j-1}(t) \approx 1$. Since $\gamma_{j-1}(t)$ is growing exponentially, the position of the peak changes only logarithmically with the prefactor $N\mu$. Changes in μ also affect the dynamics through the initial rise in frequency of

novel genotypes due to recurrent mutations; see Eq. (3).

Another factor that affects seed times is recombination. HIV recombines via template switching following the coinfection of one target cell by several virus particles (Levy *et al.*, 2004). In chronic infection, coinfection occurs with a frequency of about 1% (Batorsky *et al.*, 2011; Neher and Leitner, 2010). Recombination is not modeled in the seed time prior of our inference method but can speed up escape by combining escape mutations at different epitopes. As a result, if recombination is present, seeding tends to happen earlier than our prior would suggest. If the model assumes that seeding occurs later than in reality, there is less time for an escape variant to grow to its observed frequency. Hence the estimated escape rate (growth rate) is larger than the actual escape rate to compensate for the shorter time. In Fig. 6, we compare the estimates obtained by applying our inference method to simulation data with recombination. Recombination starts to have substantial effects once coinfection exceeds a few percent. Recombination primarily affects the incorporation of more weakly selected mutations and can be ignored for very strongly selected CTL escape mutations. Recombination also has negligible effects if the mutation rates is large as is seen in panel F of Fig. 6.

3. Unobserved intermediates and compensatory mutations

The time intervals between successive samples are sometimes too large to observe the accumulation of single mutations, so the dominant genotype at one time point differs by more than one mutation from the previous. This can arise for two reasons. First, one or several unobserved genotypes may have transiently been at high frequency but been out-competed by later genotypes before the next sample was taken. Second, one escape might have required more than one mutation, for example because single mutants are not viable and a compensatory mutation is needed (Read *et al.*, 2012). Both scenarios can be accounted for in our scheme and are illustrated in Fig. 7.

Unobserved, but individually beneficial, intermediate genotypes can be included by assuming they all have the same escape rate and were seeded one from the other. There is not sufficient information to estimate more than an average escape rate for all of them. For a given set of sampled frequencies, the estimated escape rates increase as more and more intermediates are assumed. Such unobserved intermediates are common in the data from infected individuals analyzed below.

Compensatory mutations and “multiple-hit” escapes can be accounted for by replacing the single site mutation rate in Eq. (4) by the effective rate at which the viable escape mutant appears. In the simplest case where all intermediate states are lethal and mutations are independent, this rate is simply the probability μ^k , where k is the number of mutations needed. In other cases, the rates to multiple hits can be calculated using branch-

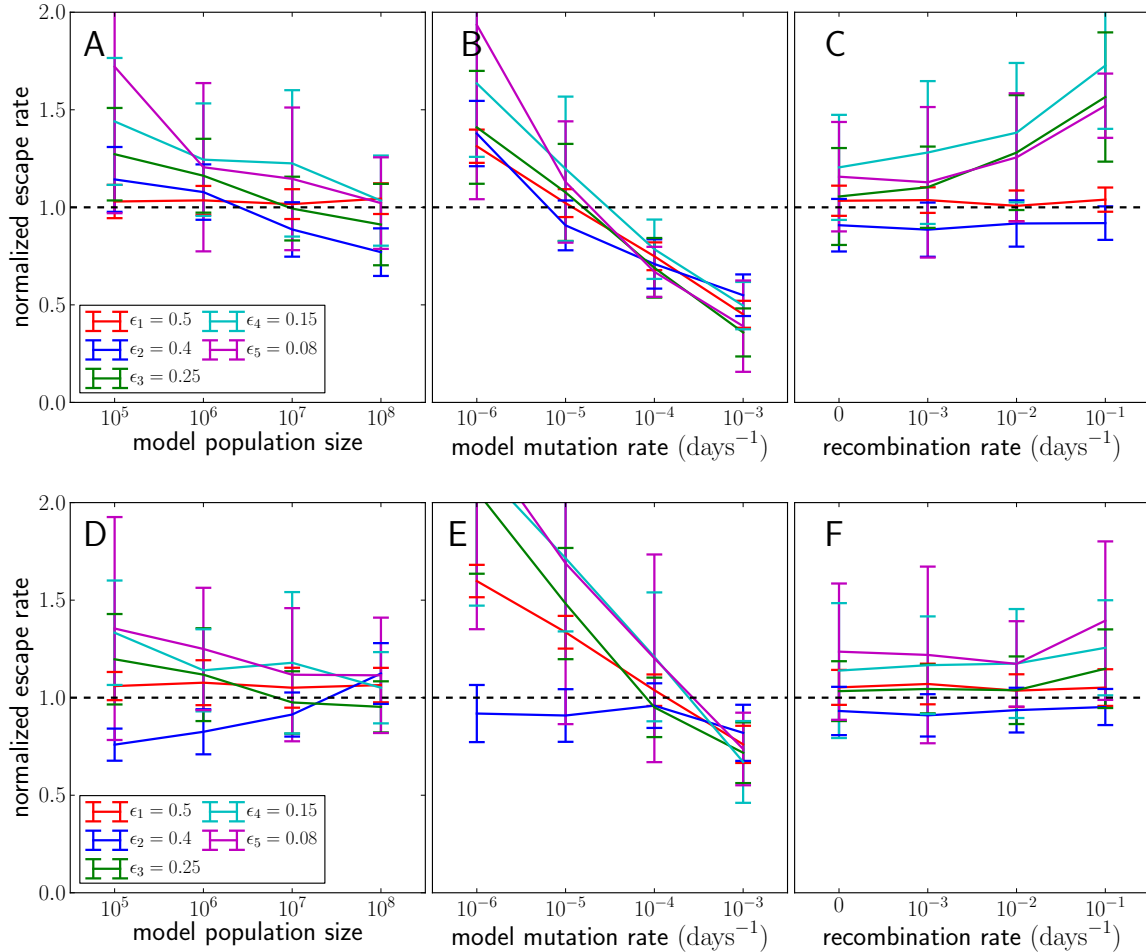


Figure 6 The effect of assuming the wrong population parameters on the escape rate estimates. To quantify the robustness against wrong assumptions, we simulate escape dynamics with parameters different from those assumed in the escape rate estimation. Panels A-C show simulations with $N = 10^7$ and $\mu = 10^{-5}$ per day, while panels D-F use a ten-fold higher mutation rate $\mu = 10^{-4}$. In panels C and F, the simulated recombination rate varies as shown. A & D) Assuming a too small population size results in estimates that are too large. The effect is more pronounced at lower mutations rates. B) Similarly, if the mutation rate is assumed too large, the estimated seeding of multiple mutants occurs too early and the estimates of escape rates are too low. Note that assuming the correct rates ($\mu = 10^{-5}$ in B and $\mu = 10^{-4}$ in F) results in unbiased estimates. C & F) If the population recombines, the actual seed times are smaller than those estimated by the fitting routine. To compensate for the shorter time interval during which the escape variant rises, the estimates of escape rates are larger than the actual escape rates at least at low mutations rates. For high mutations rates, recombination is less important since additional mutations are more efficient at producing multiple mutants than recombination. Mean and standard deviation at each point are calculated from 100 independent simulations.

ing process approximations (Neher and Shraiman, 2011; Weissman *et al.*, 2009). The choice of the relevant effective mutation rate for complex escapes must be made on a case-by-case basis. The effective mutation rate of a multiple-hit escape will often be low enough that its seed time is not very well constrained. If, for example, the population size is $N = 10^8$ and the effective mutation rate is 10^{-10} , the seed time distribution has a width of more than 100 days. Given this weak constraint, more data are required in order to estimate the escape rate accurately; see Fig. 7.

E. Immune escape in HIV-infected patients

CTL escape was characterized in detail in the patients CH58, CH40, and CH77 (Goonetilleke *et al.*, 2009; Salazar-Gonzalez *et al.*, 2009) and further analyzed in Ganusov *et al.* (Ganusov *et al.*, 2011). Sequences were obtained by single genome amplification followed by traditional sequencing. The data are sparser and less densely sampled than most of the artificial examples analyzed above, so any estimates are necessarily rather imprecise. Furthermore, we do not know exactly when infection occurred or CTL selection started. The days given in the

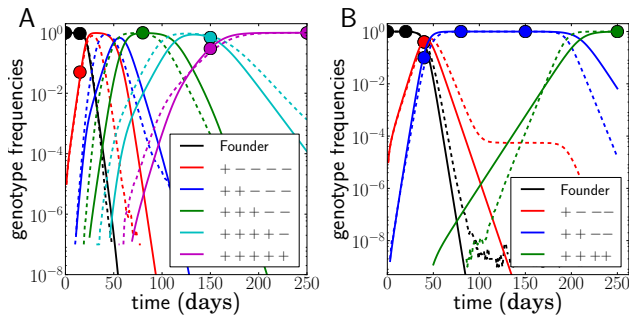


Figure 7 Unobserved intermediates and compensatory mutations. Panel A shows a scenario where the genotype with only 2 escape mutations (blue) was not observed even though this genotype was transiently at high frequencies. We fit this scenario by assuming both mutations have the same escape rate but occur sequentially ($N = 10^7$, $r = 0$, $\mu = 10^{-5}$). Panel B shows a scenario where escape mutations 3 and 4 only occur together and any genotype containing only one of the two mutations is not viable. Hence the effective mutation rate into the genotype is $\mu^2 = 10^{-10}$ and the waiting time for this genotype is longer. Note that the population size is $N = 10^9$ in this example ($r = 0$, $\mu = 10^{-5}$). The last escape only appears once the previous escape mutations have reached frequency one, and the seeding time is quite variable.

above papers are relative to the date of identification of the patient as being HIV infected. It has been estimated that in a chronically infected patient, there are a total of around 4×10^7 infected cells (Haase *et al.*, 1996). Hence, the population size is $N \approx 10^7$ but might be larger during peak viremia or smaller due to bottleneck effects or the myriad of factors influencing patient-to-patient variation in viral load. We determined posterior distributions for population sizes ranging from $N = 10^5$ to $N = 10^8$. The mutation rate was set to 10^{-5} per day (Mansky and Temin, 1995). This value is appropriate if only one escape mutation per epitope is available. If escape can happen in many different ways, a higher rate of about $\mu = 10^{-4}$ per day should be used and we repeated the estimation with $\mu = 10^{-4}$ finding similar results, see below. Both of these scenarios are observed (Henn *et al.*, 2012). Recombination in HIV occurs but is not modeled here since its rate is low (Batorsky *et al.*, 2011; Neher and Leitner, 2010), and it is expected to be less relevant for the strong escapes in large populations. In large populations, recurrent mutation is often more effective at accumulating escape mutations than recombination between two rare variants. Nevertheless, the neglect of recombination can lead to overestimation of escape rates; see above. Lastly, we assume that infection occurred $\tau = 20$ days before the patient was identified and the viral population sampled (Goonetilleke *et al.*, 2009).

For each patient, we initially considered all nonsynonymous mutations that are eventually sampled at high frequency as potential candidates for sequential escape mutants. Nearby mutations in the same epitope were

combined into one escape. We refined this list of candidates by considering only time points early in infection that were sampled with more than 5 genomes per time point and only the first 3-6 earliest strong escapes. All samples used had between 7 and 15 sequences. The frequencies of these escape mutations and their linkage into multi-locus genotypes in the 5' and 3' half of the genome, which were sequenced independently, can be easily determined from the alignment provided in Salazar-Gonzales *et al.* (Salazar-Gonzalez *et al.*, 2009). Linkage information between the 5' and 3' half genomes is missing but can in all cases be imputed using the assumption of sequential escapes. We ignored mutations whose frequency does not increase monotonically such as pol80 in subject CH40. Later in infection, there is extensive non-synonymous diversity and it is not feasible to fit a time course for most of these mutations.

In CH40 we considered samples at time points $t = 0, 16, 45, 111,$ and 181 days and identified escape in six epitopes; the first escape occurs in nef185, followed by three indistinguishable escapes at gag113, gag389, and vpr74 and two additional escapes in vif161 and env145. Following Ganusov *et al.* (Ganusov *et al.*, 2011) the number in the epitope name refers to the beginning of the 18-mer peptide covering the epitope. The mutation at env145 was not analyzed in Ganusov *et al.* (Ganusov *et al.*, 2011) and 145 is simply the number of the mutated amino acid in gp120. The indistinguishable escapes gag113, gag389, and vpr74 are treated as described in section 2.4.3 on unobserved intermediates (all three escapes are assumed to have identical escape rates and only their seed times are varied). Note that the fifth escape at epitope vif161 shows almost the same escape pattern as the three indistinguishable escapes preceding it. The escape rates of gag113, gag389, vpr74 and vif161 should therefore be interpreted with care. In CH58 we considered samples at time points $t = 0, 9, 45,$ and 85 days and identified four escapes; the first escape is at env581 and the second at env830, followed by nef105 and gag236. In CH77 we considered samples at time points $t = 0, 14,$ and 32 days and identified four escapes, namely the first escape in tat55 and subsequent escapes in env350, nef17 and nef73.

Given the above assumptions, we obtained estimates for the seed time and escape rate of each mutation. For each patient, we obtained initial estimates using a naïve single epitope fit for each mutation; then, we iterated our multi-epitope fitting model five times. Next, we obtained posterior distributions for the escape rates, all shown in Fig. 8, by performing a Markov chain Monte Carlo simulation using the likelihood function given in Eq. (5). After obtaining our estimates, we randomly changed the escape rates in increments of ± 0.01 and the seed times by ± 1 , reevaluated the likelihood, and accepted the change with probability $\exp(\Delta)$, where Δ is the change in likelihood. The resulting Markov chain was run for 10^6 steps with samples taken every 1000 steps.

Figure 8 shows the posterior distributions of the escapes rate for different epitopes in the three patients

evaluated assuming a mutation rate $\mu = 10^{-5}$ per day. Larger population sizes result in smaller estimates of the escape rates, as expected from Fig. 6A. The posterior distribution for the first escapes are often very tight, but they depend on the time of the onset of CTL selection, which we have set here to $T = 20$ days prior to the first sample. If we assume that the time of the onset of CTL selection coincided with the first sample (i.e., $T = 0$), the estimates of escape rates of the first epitope ϵ_1 are around 0.9, while later escapes are almost not sensitive to the choice of T .

While the posterior distributions of escape rates of subsequent escape rates are quite broad, they nevertheless suggest that escape rates can be substantially higher than previously estimated (Asquith *et al.*, 2006; Ganusov *et al.*, 2011). Furthermore, the escape rate is not obviously negatively correlated with the time of emergence during acute infection with HIV-1, at least for the earliest four to six escapes. The underlying reason for this is that selection on a late escape is only active after the successful multiple mutant has been produced. In previous single epitope estimates, selection was allowed to act on the mutant frequency from the very beginning, resulting in a reduced estimate of the escape rate. Figure 8 also shows the inferred trajectories for the most likely parameter combination for patient CH40. One clearly sees the rapid rise and fall of multiple genotypes between the second and third time point. Given the large number of genotypes involved and the little data available, the escape rates estimated for this case are rather noisy. But this analysis clearly shows that strong selection is necessary to bring four mutations to fixation in just a few weeks. We repeated the analysis of the patient data assuming a mutation rate of $\mu = 10^{-4}$ and show the results in Fig. 9. The overall picture is similar to what we found for $\mu = 10^{-5}$ per day, but escape rates tend to be lower.

II. DISCUSSION

We have suggested a way to infer viral escape rates from time series data sparsely sampled from the evolutionary dynamics of asexual or rarely sexual populations such as HIV. We exploit the sequential nature at which escape mutations accumulate, which allows us to constrain the times at which new escape mutations arose. These constraints regularize the inference to a large extent, but additional stability is gained by prioritizing small escape rates through an exponential prior.

Rates of single escape mutations have so far been estimated by comparing the time series data to a model that assumes logistic growth of the mutation with a constant rate. This approach has been used to analyze the intra-patient dynamics of recombinant HIV (Liu *et al.*, 2002), drug resistance (Bonhoeffer *et al.*, 2002; Paredes *et al.*, 2009), and CTL escape dynamics (Asquith *et al.*, 2006; Asquith and McLean, 2007; Ganusov and De Boer, 2006; Ganusov *et al.*, 2011; Petracic *et al.*, 2008b). While

these methods work well if each mutation is sampled multiple times at intermediate frequencies, they provide very conservative lower bounds when data is sparse. Furthermore, they ignore the effects of competition between escapes at different epitopes and assume that each epitope can be treated independently. Since the recombination frequency in HIV is low (Batorsky *et al.*, 2011; Josefsson *et al.*, 2011; Neher and Leitner, 2010), this can be a poor approximation. Our method improves on previous methods on both of these counts. We explicitly model the competition between escape mutations. This competition places constraints on the times at which genotypes with multiple escapes first arise (double mutants arise only after the single mutants), which makes the inference more robust and the lower bound tighter.

A related method to estimate CTL escape rates has been proposed by Levinyang (Levinyang, 2013), who modeled multiple escape mutations by an escape graph that is traversed by the viral population. Combining these two approaches, intra-epitope competition as modeled in (Levinyang, 2013) and the between epitope competition studied here would be an interesting extension. Similar ideas have been developed in the context of mutations in cancer or evolution experiments (Illingworth and Mustonen, 2012).

While previous methods neglect interactions between epitopes altogether – equivalent to assuming very rapid recombination – our method ignores recombination during the inference. By comparison with simulations that include recombination, we have shown that neglecting recombination can result in overestimation of the escape rates by roughly 30% at plausible recombination rates of 1% (Batorsky *et al.*, 2011; Neher and Leitner, 2010). We also show that neglecting recombination is less of a problem at higher mutation rates. Note that neglecting recombination cannot explain the larger escape estimates compared to previous studies. For patient CH58 we find escape rates that are up to three-fold higher than earlier estimates (Ganusov *et al.*, 2011), while we never see such a big deviation in our sensitivity analysis. Furthermore, the errors made when neglecting recombination for rapid early escapes are comparable to the uncertainties that result from infrequent sampling or more severe deviations of the model from reality, such as time variable CTL activity.

Reanalysis of CTL escape data from HIV using our method suggests that CTL escapes are substantially more rapid than previously thought. Even with a large prior against high escape rates ($\Phi = 10$), we estimate that the escape rates of the first 4-6 escapes are on the order of 0.3 – 0.4 per day. The estimates at large population sizes are fairly insensitive to the prior for population sizes of 10^6 or larger. Early in infection, it is plausible to assume that the relevant size is $N = 10^7$ (Boltz *et al.*, 2012; Coffin, 1995; Perelson *et al.*, 1997). If population sizes are small, relaxing the prior against high escape rates results in larger estimates, which further supports our finding that escape rates are often large and compe-

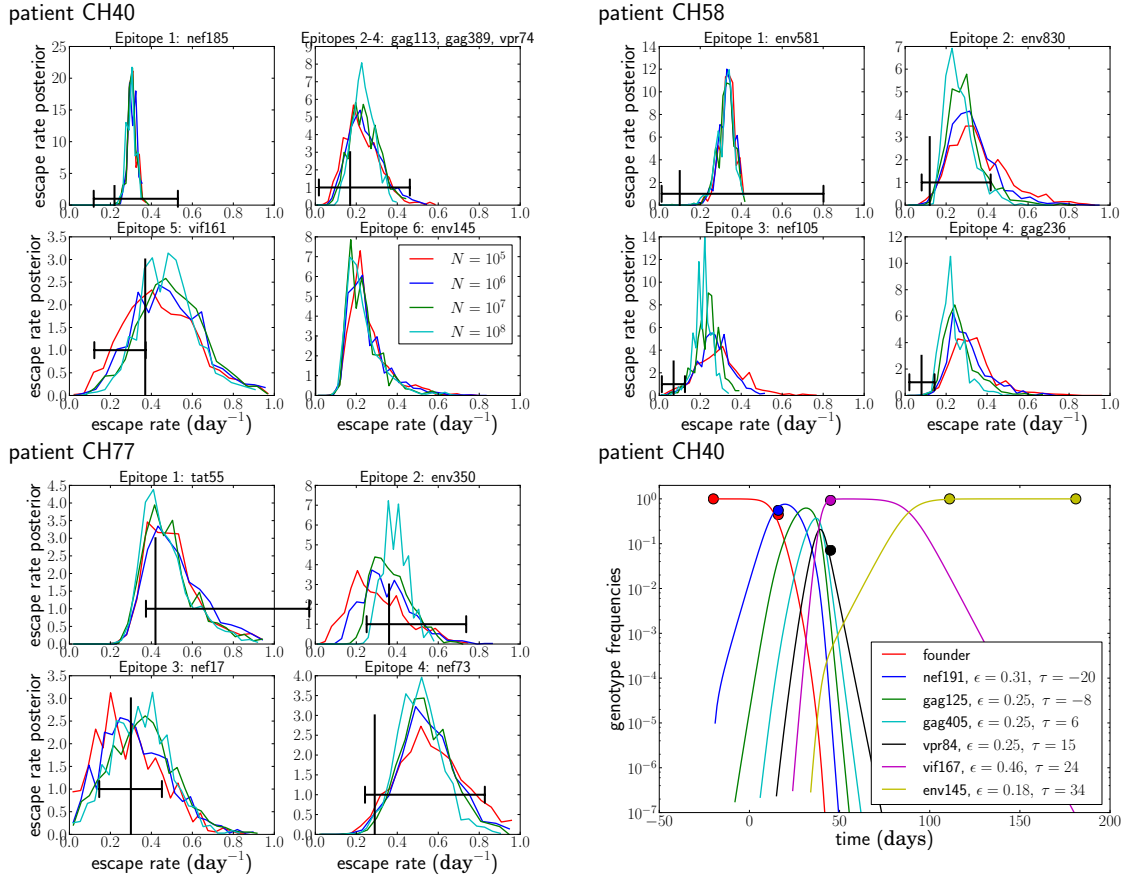


Figure 8 The posterior distribution of the escape rates for different population sizes. It is assumed that CTL selection starts 20 days prior to the date of identification, and the fitness prior has weight $\Phi = 10$. The black vertical and horizontal lines indicate the estimates and confidence intervals obtained in Ganusov et al (Ganusov *et al.*, 2011). Note that the mutation env145 in CH40 was not analyzed in Ganusov et al (Ganusov *et al.*, 2011). The lower right panel shows the most likely genotype trajectories for patient CH40 with parameters $N = 10^7$ and $\mu = 10^{-5}$. Each curve is labeled by an epitope, but should be understood as the frequency of the genotype that has escaped at this and all previous epitopes. Note that no data is available to differentiate epitopes gag113, gag389 and vpr74. For those, we assume an arbitrary order and equal escape rates as explained in Sec. 2.4.3.

tion between escapes needs to be modeled. Given the sparse data, we can only estimate parameters of simple models and have to neglect many complicating features of HIV biology. Among other factors, the rate at which escape mutations are selected depends on the overall R_0 of the infection and CTL selection is probably time variable (Ganusov *et al.*, 2011). The estimated parameters therefore represent time averaged effect escape rates.

The timing of escape has been shown to depend on epitope entropy and immunodominance (Liu *et al.*, 2013). However, we modeled only the first four to six escapes in each patient from which rather little information about differential timing can be obtained. In the case of CH77, the first four escapes occurred within a month from the identification of the patient. In patient CH58, it took roughly three months for four escapes to spread and the estimated escape rates are lower as expected. In the case of CH40 four of the six escapes show almost or completely indistinguishable escape patterns and we have little power to differentiate the escape rates at epitopes

gag113, gag389, vpr74 and vif161. Hence any meaningful correlation with immunological features and epitope sequence conservation, i.e., low entropy, requires more data.

The proposed method to analyze multi-locus time series of adaptive evolution could be useful in many contexts where the genotypic compositions of large populations of viruses or cells can be monitored over time. Whenever mutations occur rapidly enough that they compete with each other, this competition has to be accounted for in the analysis. Outside of virus evolution, possible applications include the development of cancer and microbial evolution experiments.

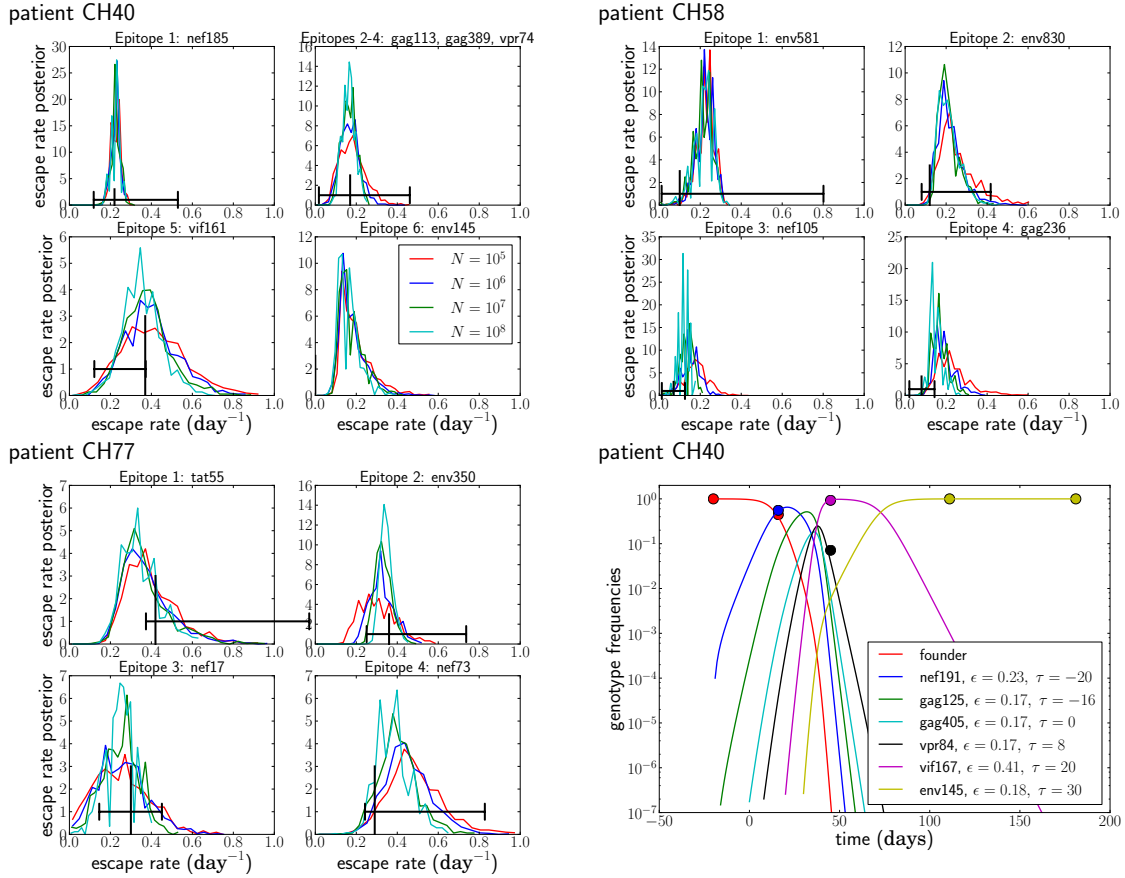


Figure 9 Posterior distributions of escape rate assuming a mutation rate $\mu = 10^{-4}$ per day. See Fig. 8 for other details.

III. MATERIALS & METHODS

A. Data Preparation.

Our fitting method uses counts k_{ij} of genotypes g_j at time points t_i to infer escape rates of individual mutations. The procedure used to obtain successive genotype counts from sequence data sampled from patients is outlined in the text. As input data, our analysis scripts expect a white-space delimited text file with a format shown in Table I. In addition, a separate file with the total number of sequences at each time point can be provided. This file is expected to have the same format as the matrix with the genotype counts; see Table I. In absence of such a file, the sample sizes at each time point are obtained by summing the genotype counts.

To test our method, artificial data $k_{ij} = k(g_j, t_i)$ were obtained from simulated trajectories (generated by FF-PopSim) by binomial sampling (with size n_i) at specified time points t_i . Trajectory generation and sampling are implemented in the file `model_fit/ctlutils.py` at <http://git.tuebingen.mpg.de/ctlfit>; see below.

time [days]	founder	env581	env830	nef105	gag236
9	5	2	0	0	0
45	0	0	5	3	0
85	0	0	0	0	8

Table I Format of input data: The escape mutations are ordered first by the time of first observation and then by abundance. Each entry in the table in a particular column reports the number of times a sequence is observed containing the escape of that column and **all** previous escape mutations.

1. Sequence data

The HIV sequences for patients CH40, CH58 and CH77 were downloaded from http://www.hiv.lanl.gov/content/sequence/HIV/USER_ALIGNMENTS/Salazar.html (Salazar-Gonzalez *et al.*, 2009).

B. Inference.

The inference procedure consists of *initial guessing*, *sequential addition of escapes*, *multi-dimensional refinement*, and estimation of *posterior distributions*. The im-

plementation can be found in `src/ctl_fit.py`, with the C code for the likelihood calculation in `src/cfit.cpp`.

Initial guesses. We produce initial guesses by single epitope modeling. The frequency of each escape mutation, ν_j , grows logistically with the escape rate (Ganusov *et al.*, 2013). We expect that only the frequency of the first escape mutation is significantly affected by mutational input, since it receives input from the abundant founder sequence, while the later escapes only receive mutational input from the previously escape genotype, which is still rare when the novel escape arises. Hence we only model the mutational dynamics of the first escape. In a single epitope model, the frequency of the founder variant is one minus the frequency of the escape variant. The frequency of the escape variant increases by $\mu(1 - \nu_1)$ per day due to mutations from the founder, and decreases by $\mu\nu_1$ due to further mutations to additional escapes. Combined with the logistic growth, the dynamics of ν_1 is described by

$$\dot{\nu}_1(t) = \epsilon_1\nu_1(1 - \nu_1) + \mu[1 - 2\nu_1]. \quad (6)$$

with initial condition $\nu_1(0) = 0$. Note the difference between the allele frequency ν , which refers to a particular escape mutation, and γ , which corresponds to frequencies of particular multi-epitope genotypes. The above ODE has the solution

$$\nu_1(t) = \frac{1}{2\epsilon_1}[\epsilon_1 - 2\mu + R \tanh(\frac{\alpha + t}{2}R)] \quad (7)$$

where $R = \sqrt{\epsilon_1^2 + 4\mu^2}$ and $\alpha = \frac{4\mu - 2\epsilon_1}{4\mu^2 + \epsilon_1^2}$ (Ganusov *et al.*, 2013). The escape rate ϵ_1 is determined by maximizing the likelihood (Eq. (5)) using `fmin` from `scipy` (Oliphant, 2007).

The seed time τ_j of subsequent escape mutants g_j is determined by maximizing the seed time prior $Q(\tau_j|\gamma_{j-1})$ defined in Eq. (4) using the previously determined γ_{j-1} . The frequencies of mutations are assumed to follow a logistic trajectory since the genotype from which they receive mutational input is itself still at low frequency:

$$\nu_j(t) = \frac{e^{\epsilon_j(t-\tau_j)}}{e^{\epsilon_j(t-\tau_j)} + N\epsilon_j} \quad j > 1. \quad (8)$$

Again, we maximize the posterior probability, Eq. (5), to obtain an initial estimate of ϵ_j .

Sequential addition of escapes. Given the initial estimates for the first escape, we now add subsequent escapes to the multi-epitope model, which is formulated in terms of genotype counts k_{ij} and frequencies $\gamma_j(t)$. Note that the interpretation of genotype counts depends on how many epitopes are modeled. For example, if we model epitopes $1, \dots, j$ out of a total of L epitopes, counts for genotype j are $k_{ij} = \sum_{l=j}^L k_{il}$, i.e., we ignore all later escapes.

If the added escape is unique, i.e., no other escape mutation has the exact same temporal pattern, we calculate the likelihood on a 21×31 grid of escape rates and seed times; comp. Fig. 4. The grid spans values between 0 and twice the initial estimate for both the seed time and the escape rate. The most likely combination of seed time and escape rate is chosen, and the procedure is repeated with the next epitope.

If multiple epitopes exhibit the same temporal pattern, we add them all at once, constrain their escape rates to be equal, and assume they emerged in the order listed in the genotype matrix. Since we now have to optimize one joint escape rate and multiple seed times, we do not map the likelihood surface exhaustively but rather perform a greedy search. We examine next-neighbor moves with steps $\delta\tau = \pm 1$ day and $\delta\epsilon = \pm 0.02$ per day, moves which change all seed times by $\delta\tau$, and 20 moves in which all seed times and escape rates are changed by $\delta\tau$ and $\delta\epsilon$ with random sign; the step that maximizes the likelihood is accepted. This is repeated until no favorable move is found and further repeated with $\delta\epsilon = 0.01$ and 0.001 per day.

Refinement. We then iterate sequentially over every epitope and optimize its seed times and escape rates as described above, but with all other epitopes part of the multi-epitope model. This typically leads to rather small adjustments and converges rapidly.

Posterior distributions. To determine the posterior distribution of the escape rates, we attempt to change all seed times and escape rates by $\delta\tau = \pm 1$ day and $\delta\epsilon = \pm 0.01$ per day with random sign. The move is accepted with probability $\max(1, \exp(-\Delta))$, where Δ is the difference in log-likelihood before and after the change. We sample this Markov chain every 1000 moves and thereby map the posterior distribution of seed times and escape rates.

C. Usage

Availability All source code and scripts are available at <http://git.tuebingen.mpg.de/ctlfit>.

Building The part of our method that is implemented in C and the python bindings can be built using `make` and the Makefile provided in the `src` directory. Prerequisites for building are `python2.7`, `scipy`, `numpy`, `swig`, and a `gcc` compiler.

Fitting Given a text file with genotype counts specified as shown in table I, fitting is performed by calling the script `fit_escapes.py` with python. Parameters can be

set via command line arguments:

```
python fit_escapes.py --input datafile (9)
```

where `--input` specifies the file with the genotype counts. Other parameters can be modified in a similar manner. Running the script with the option `--help` prints a list of all parameters. The estimated escape rates and seed times as well as the sampled posterior distribution will be saved in the directory `fit_escapes_output`, unless otherwise specified.

Disclosure/Conflict-of-Interest Statement

The authors declare that the research was conducted in the absence of any commercial or financial relationships that could be construed as a potential conflict of interest.

Acknowledgements

We are grateful for stimulating discussions with F. Zanini. This work is supported by the ERC starting grant HIVEVO 260686 (RAN) and in part by the National Science Foundation under Grant No. NSF PHY11-25915. This work was performed under the auspices of the US Department of Energy under contract DE-AC52-06NA25396 and supported by NIH grant AI028433, the National Center for Research Resources and the Office of Research Infrastructure Programs (ORIP) through grant OD011095 (ASP).

References

- Asquith, B., C. T. T. Edwards, M. Lipsitch, and A. R. McLean, 2006, *PLoS Biol* **4**(4), e90.
- Asquith, B., and A. R. McLean, 2007, *Proc Natl Acad Sci USA* **104**(15), 6365.
- Basu, D., 1977, *J Am Stat Assoc* **72**(358), 355.
- Batorsky, R., M. F. Kearney, S. E. Palmer, F. Maldarelli, I. M. Rouzine, and J. M. Coffin, 2011, *Proc Natl Acad Sci USA* **108**(14), 5661.
- Boltz, V. F., Z. Ambrose, M. F. Kearney, W. Shao, V. N. KewalRamani, F. Maldarelli, J. W. Mellors, and J. M. Coffin, 2012, *J Virol* **86**(23), 12525.
- Bonhoeffer, S., A. D. Barbour, and R. J. D. Boer, 2002, *Proc Biol Sci* **269**(1503), 1887.
- Coffin, J. M., 1995, *Science* **267**(5197), 483.
- Desai, M. M., and D. S. Fisher, 2007, *Genetics* **176**(3), 1759.
- Fernandez, C. S., I. Stratov, R. D. Rose, K. Walsh, C. J. Dale, M. Z. Smith, M. B. Agy, S.-L. Hu, K. Krebs, D. I. Watkins, D. H. O'connor, M. P. Davenport, *et al.*, 2005, *J Virol* **79**(9), 5721.
- Fischer, W., V. V. Ganusov, E. E. Giorgi, P. T. Hraber, B. F. Keele, T. Leitner, C. S. Han, C. D. Gleasner, L. Green, C.-C. Lo, A. Nag, T. C. Wallstrom, *et al.*, 2010, *Plos ONE* **5**(8), e12303, URL <http://www.plosone.org/article/info%253Adoi%252F10.1371%252Fjournal.pone.0012303>.
- Ganusov, V. V., and R. J. De Boer, 2006, *PLoS Comput Biol* **2**(3), e24.
- Ganusov, V. V., N. Goonetilleke, M. K. P. Liu, G. Ferrari, G. M. Shaw, A. J. McMichael, P. Borrow, B. T. Korber, and A. S. Perelson, 2011, *J Virol* **85**(20), 10518.
- Ganusov, V. V., R. A. Neher, and A. S. Perelson, 2013, *J Stat Mech-Theory E* **2013**(01), P01010.
- Goonetilleke, N., M. K. P. Liu, J. F. Salazar-Gonzalez, G. Ferrari, E. Giorgi, V. V. Ganusov, B. F. Keele, G. H. Learn, E. L. Turnbull, M. G. Salazar, K. J. Weinhold, S. Moore, *et al.*, 2009, *J Exp Med* **206**(6), 1253.
- Haase, A. T., K. Henry, M. Zupancic, G. Sedgewick, R. A. Faust, H. Melroe, W. Cavert, K. Gebhard, K. Staskus, Z.-Q. Zhang, P. J. Dailey, H. H. Balfour, *et al.*, 1996, *Science* **274**(5289), 985.
- Henn, M. R., C. L. Boutwell, P. Charlebois, N. J. Lennon, K. A. Power, A. R. Macalalad, A. M. Berlin, C. M. Malboeuf, E. M. Ryan, S. Gnerre, M. C. Zody, R. L. Erlich, *et al.*, 2012, *PLoS Pathog* **8**(3), e1002529, URL <http://dx.doi.org/10.1371/journal.ppat.1002529>.
- Illingworth, C. J. R., and V. Mustonen, 2012, *Bioinformatics* **28**(6), 831.
- Josefsson, L., M. S. King, B. Makitalo, J. Brännström, W. Shao, F. Maldarelli, M. F. Kearney, W.-S. Hu, J. Chen, H. Gaines, J. W. Mellors, J. Albert, *et al.*, 2011, *Proc Natl Acad Sci USA* **108**(27), 11199.
- Keele, B. F., E. E. Giorgi, J. F. Salazar-Gonzalez, J. M. Decker, K. T. Pham, M. G. Salazar, C. Sun, T. Grayson, S. Wang, H. Li, X. Wei, C. Jiang, *et al.*, 2008, *Proc Natl Acad Sci USA* **105**(21), 7552.
- Kepler, T. B., and A. S. Perelson, 1995, *Proc Natl Acad Sci USA* **92**(18), 8219.
- Leviyang, S., 2013, *Genetics*, ahead of print .
- Levy, D. N., G. M. Aldrovandi, O. Kutsch, and G. M. Shaw, 2004, *Proc Natl Acad Sci USA* **101**(12), 4204.
- Li, B., A. D. Gladden, M. Altfeld, J. M. Kaldor, D. A. Cooper, A. D. Kelleher, and T. M. Allen, 2007, *J Virol* **81**(1), 193.
- Liu, M. K., N. Hawkins, A. J. Ritchie, V. V. Ganusov, V. Whale, S. Brackenridge, H. Li, J. W. Pavlicek, F. Cai, M. Rose-Abrahams, F. Treurnicht, P. Hraber, *et al.*, 2013, *J Clin Invest* **123**(1), 380, ISSN 0021-9738, PMID: 23221345 PMID: PMC3533301, URL <http://www.ncbi.nlm.nih.gov/pmc/articles/PMC3533301/>.
- Liu, S.-L., J. E. Mittler, D. C. Nickle, T. M. Mulvania, D. Shriner, A. G. Rodrigo, B. Kosloff, X. He, L. Corey, and J. I. Mullins, 2002, *J Virol* **76**(21), 10674.
- Mansky, L. M., and H. M. Temin, 1995, *J Virol* **69**(8), 5087.
- Markowitz, M., M. Louie, A. Hurley, E. Sun, M. Di Mascio, A. S. Perelson, and D. D. Ho, 2003, *J Virol* **77**(8), 5037.
- McMichael, A. J., P. Borrow, G. D. Tomaras, N. Goonetilleke, and B. F. Haynes, 2009, *Nat Rev Immunol* **10**(1), 11.
- Neher, R. A., and T. Leitner, 2010, *PLoS Comput Biol* **6**(1), e1000660.
- Neher, R. A., and B. I. Shraiman, 2011, *Genetics* **188**, 975.
- Oliphant, T., 2007, *Comput Sci Eng* **9**(3), 10.
- Paredes, R., M. Sagar, V. C. Marconi, R. Hoh, J. N. Martin, N. T. Parkin, C. J. Petropoulos, S. G. Deeks, and D. R. Kuritzkes, 2009, *J Virol* **83**(4), 2038.
- Perelson, A. S., P. Essunger, and D. D. Ho, 1997, *AIDS* **11 Suppl A**, S17.
- Perelson, A. S., A. U. Neumann, M. Markowitz, J. M. Leonard, and D. D. Ho, 1996, *Science* **271**(5255), 1582.
- Petravic, J., L. Loh, S. J. Kent, and M. P. Davenport, 2008a, *J Virol* **82**(8), 4091.
- Petravic, J., R. M. Ribeiro, D. R. Casimiro, J. J. Mattapallil, M. Roederer, J. W. Shiver, and M. P. Davenport, 2008b, *J*

- Virology **82**(23), 11589.
- Read, E. L., A. A. Tovo-Dwyer, and A. K. Chakraborty, 2012, Proc Natl Acad Sci USA **109**(48), 19727.
- Salazar-Gonzalez, J. F., M. G. Salazar, B. F. Keele, G. H. Learn, E. E. Giorgi, H. Li, J. M. Decker, S. Wang, J. Baalwa, M. H. Kraus, N. F. Parrish, K. S. Shaw, *et al.*, 2009, J Exp Med **206**(6), 1273.
- Seki, S., and T. Matano, 2012, Front. Microbio. **2**, 267.
- Silva, J. d., 2012, Genetics **190**(3), 1087, ISSN 0016-6731, 1943-2631, PMID: 22209906, URL <http://www.genetics.org/content/190/3/1087>.
- Sunkker, M., A. G. Busetto, E. Numminen, J. Corander, M. Foll, and C. Dessimoz, 2013, PLoS Comput Biol **9**(1), e1002803.
- Weissman, D. B., M. M. Desai, D. S. Fisher, and M. W. Feldman, 2009, Theor Pop Bio **75**(4), 286.
- Zanini, F., and R. A. Neher, 2012, Bioinformatics **28**(24), 3332.